

# Heavy Meson Production in Proton-Nucleus Reactions with Empirical Spectral Functions\*

A. Sibirtsev, W. Cassing and U. Mosel  
Institut für Theoretische Physik, Universität Giessen  
D-35392 Giessen, Germany

January 6, 2018

PACS: 24.10.-i; 24.30.-v; 24.50.+g; 25.40.-h

## Abstract

We study the production of  $K^+$ ,  $\rho$ ,  $\omega$  and  $\phi$  mesons in  $p + {}^{12}\text{C}$  reactions on the basis of empirical spectral functions. The high momentum, high removal energy part of the spectral function is found to be negligible in all cases close to the absolute threshold. Furthermore, the two-step process ( $pN \rightarrow \pi NN$ ;  $\pi N \rightarrow N + K^+, \rho, \omega, \phi$ ) dominates the cross section at threshold energies in line with earlier calculations based on the folding model.

---

\*Supported by Forschungszentrum Jülich

# 1 Introduction

The production of heavy mesons in proton-nucleus reactions even below the free nucleon-nucleon threshold is of specific interest [1, 2, 3, 4, 5] as one hopes to learn about cooperative nuclear phenomena, high momentum components of the nuclear wavefunction or in-medium modifications of the mesons themselves. Furthermore, a precise knowledge of the meson production channels in  $p + A$  collisions is a necessary step towards a microscopic understanding of meson production in nucleus-nucleus collisions, where in-medium modifications should be enhanced due to the higher baryon densities achieved [6, 7]. Especially the production channels for the vector mesons is of particular interest because their abundancy can be controlled by dilepton spectroscopy independently. A possible 'softening' of the  $\rho$  meson at high baryon density [8] as possibly indicated by  $e^+e^-$  and  $\mu^+\mu^-$  data [9, 10, 11, 12] should also show up in the  $\rho^0$  production on nuclei and could be controlled by the  $\pi^+\pi^-$  invariant spectrum.

So far, the production of  $\eta$  and  $K^+$  mesons on nuclei has been addressed, both theoretically [13, 14, 15, 16, 17, 18] and experimentally [19, 20, 21, 22, 23, 24], whereas only a few model studies on the production of  $K^-$  and  $\rho, \omega, \phi$  mesons are available [15, 25]. Most of the former approaches - though partly using the experimental momentum distribution for the target of interest - employ a quasi-free dispersion relation for the struck target nucleon and thus come in conflict with the A-body energy-momentum conservation close to the absolute threshold because the struck target nucleon is off-shell.

Experimental information about the nucleon momentum *and* energy distribution is available from  $(e, e'p)$  reactions [26]. The data show in addition to the 'mean-field' spectral function a high momentum, high energy component which might be attributed to nucleon-nucleon correlations with high relative but low center-of-mass momenta [27]. The influence of this 'correlation' component on heavy meson production in proton-nucleus collisions is of particular interest in our present study as well as the role of primary and secondary (pion induced) reaction channels.

Our paper thus is organized as follows: In Section 2 we describe our approach for meson production in proton induced reactions with spectral functions and discuss its ingredients, i.e. the spectral function itself, the elementary production cross sections in  $pN$  and  $\pi N$  collisions, the effective number of collisions as well as meson reabsorption effects in Section 3. By discarding possible in-medium effects we then present in Section 4 our results for  $p + {}^{12}\text{C}$  reactions for  $K^+, \rho, \omega$  and  $\phi$  mesons as a function of the beam energy  $T_0$  with their channel decompositions. A summary and discussion of open problems concludes this paper in Section 5.

## 2 Reaction model for proton-nucleus collisions

In terms of a multiple scattering theory the particle production in proton-nucleus collisions can be described as an incoherent sum of two-body interactions [28, 29, 30]. However, the individual interactions in nuclear matter might differ from those in free space due to the average interaction of the collision partners with the surrounding nuclear medium [31].

The first term from the multiple scattering theory we denote as the 'direct' or 'one-step' production process. Furthermore, neglecting the medium effects on the reaction partners, this approach corresponds to the 'impulse approximation' which can be applied whenever the relevant energy scale is large compared to the nuclear binding energy. Within the single-scattering approximation the Lorentz-invariant differential cross section for meson production in  $p + A$  collisions then can be written as

$$E_M \frac{d^3 \sigma_{pA \rightarrow MX}}{d^3 p_M} = \frac{N_{eff}(E_M)}{A} \int_{\Omega} d^3 q d\omega S_P(\mathbf{q}, \omega) E'_M \frac{d^3 \sigma_{pN \rightarrow MX}(\sqrt{s})}{d^3 p'_M} \quad (1)$$

with  $\sqrt{s}$  being the invariant energy of the incident proton and the struck nucleon defined as

$$s = (E_0^* + \omega)^2 - (\mathbf{p}_0^* + \mathbf{q})^2 \quad (2)$$

where  $E_0^*$ ,  $\mathbf{p}_0^*$  and  $\omega$ ,  $\mathbf{q}$  are the total energy and the momentum of the beam and target nucleon, respectively. Here the \*-indices denote the influence of the average nuclear optical potential  $U_{opt}$  which changes the kinetic energy of the incident proton as

$$T_0^* = T_0 - U_{opt}, \quad (3)$$

where  $T_0$  is the beam kinetic energy and  $E_0^* = T_0^* + m_N$ , while  $m_N$  is the nucleon mass. Note that the momentum of the incoming proton  $\mathbf{p}_0^*$  also has to be modified properly in case of vector potentials. The momentum-dependent optical potential for cold nuclear matter at normal density  $\rho_0 \approx 0.158 fm^{-3}$  is about - 70 MeV for  $p_0 = 0$ , becomes repulsive at beam energies above 300 MeV and reaches an almost constant value of 30 - 50 MeV [32, 33, 34, 35]. Thus the optical potential for the impinging proton is the first medium effect that has to be taken into account.

The primed indices in Eq. (1) denote the meson momentum and energy in the cms of the beam and the individual target nucleon, while  $E'_M d^3 \sigma_{pN \rightarrow MX} / d^3 p'_M$  is the Lorentz invariant elementary cross section for meson production from  $p + N$  collisions in free space. The factor  $N_{eff}$  accounts for the effective primary collision number as well as for the in-medium absorption of the meson when propagating through the nuclear target as described in Section 3.4. In Eq. (1) the index  $\Omega$  stands for the Pauli blocking of the final states.

The function  $S_P(q, \omega)$ <sup>1</sup> relates the momentum of the target nucleon  $q$  with its energy  $\omega$ . The free space relation,  $\omega^2 = q^2 + m_N^2$ , is no longer valid for a system of bound nucleons because they are off-shell. In the mean-field approach the average total energy of the bound nucleon is [18, 36]

$$\frac{1}{A} \sum_{j=1}^A \omega_j = \frac{M_A}{A} \simeq (m_N - \epsilon) \quad (4)$$

where  $M_A$  denotes the mass of the target while  $\epsilon$  stands for the binding energy per nucleon. Realistic spectral functions  $S_P(q, \omega)$ , as used in the present calculations, will be discussed in Section 3.1.

---

<sup>1</sup>We adopt the normalization  $\int d^3 q d\omega S_P(q, \omega) = A$ , where  $A$  denotes the target mass.

As proposed in [37, 38] the dominant contribution to subthreshold heavy meson production should arise from a two-step reaction mechanism with an intermediate pion. In accord with [13, 17] the cross sections for  $K^+$ ,  $\rho$ ,  $\omega$  and  $\phi$ -mesons from the secondary pion induced reactions are calculated as

$$E_M \frac{d^3 \sigma_{pA \rightarrow MX}}{d^3 p_M} = \frac{N_{eff}(E_M)}{A} \int_{\Omega} d^3 q \, d\omega \frac{d^3 p'_\pi}{E'_\pi} S_P(\mathbf{q}, \omega) \times E''_M \frac{d^3 \sigma_{\pi N \rightarrow MX}(\sqrt{s})}{d^3 p''_M} \frac{g_\pi}{\sigma_{tot}} \times E'_\pi \frac{d^3 \sigma_{pN \rightarrow \pi X}(\sqrt{s'})}{d^3 p'_\pi} \quad (5)$$

where the double prime indices denote the system of the intermediate pion and a target nucleon, while the single prime indices are those for the beam and the first target nucleon. Moreover,  $E_\pi d^3 \sigma_{pN \rightarrow \pi X} / d^3 p_\pi$  stands for the  $\pi$ -meson differential production cross section, which is calculated in line with (1), while  $\sigma_{tot}$  is the total proton-nucleon cross section. We note that the on-shell elementary  $\pi$ -meson production e.g. can be described within the isobar model [39, 40]. The factor  $g_\pi$  in Eq. (5) accounts for the probability that the pion interacts again with a target nucleon (cf. Section 3.4).

## 3 Ingredients of the model

### 3.1 The spectral function

The in-medium relation between the energy  $\omega$  and the momentum  $\mathbf{q}$  of the target nucleon relevant to subthreshold particle production can be defined in analogy to Guet and Prakash [41], where the energy  $E_{prod}$  (available for the meson production) is related to the incoming energy by total energy conservation as

$$E_0^* + M_A = E_{prod} + \left( M_{A-1}^2 + \mathbf{q}^2 \right)^{1/2} + E_{exc}, \quad (6)$$

where  $M_A$  and  $M_{A-1}$  are the masses of the initial and residual nuclei, respectively,  $\mathbf{q}$  is the internal momentum and  $E_{exc}$  stands for the excitation energy of the final nucleus.

The excitation energy  $E_{exc}$  now is related to the removal energy  $E_R$  as [42]

$$E_{exc} = E_R + M_A - M_{A-1} - m_N, \quad (7)$$

where  $E_R$  is the energy necessary to extract the nucleon from the nucleus. Thus

$$\omega = m_N - E_R \quad (8)$$

with  $E_R > 0$ . The probability to find a nucleon with momentum  $\mathbf{q}$  and removal energy  $E_R$  in a nucleus now is given by the nucleon spectral function  $S(q, E_R)$ . Accordingly, the function  $S_P(q, \omega)$  entering our calculations in (1),(5) can be evaluated from the spectral function  $S(q, E_R)$  by substituting Eq. (8).

The evaluation of the spectral function itself is quite an involved problem [43, 44, 45] and still a matter of discussion. In the present calculations we adopt  $S(q, E_R)$  from Sick et al. [46] obtained within the orthogonal correlated basis approach as well as a

phenomenological spectral function from Ciofi degli Atti and Simula [27], that both provide a good description of  $(e, e'p)$  reactions.

The  $S(q, E_R)$  for  $^{12}\text{C}$  from ref. [46] is shown in Fig. 1 as a function of the nuclear nucleon momentum  $q$  and removal energy  $E_R$ . In the upper part of Fig. 2 we display the spectral function up to  $E_R \approx 60$  MeV on a larger scale in order to show the 'mean-field' distribution dominated by the  $s_{1/2}$  and  $p_{3/2}$  single-particle levels at  $E_R \approx 35$  MeV and  $E_R \approx 20$  MeV, respectively. As a 'background' under the horizontal shell structure one can notice a ridge roughly along

$$E_R \simeq 45\text{MeV} - \frac{q^2}{2m_N} \quad (9)$$

leading to a total available energy for particle production

$$\omega \simeq m_N - 45\text{MeV} + \frac{q^2}{2m_N}. \quad (10)$$

This is close to the dispersion relation often used in folding model calculations.

The full spectral function up to  $E_R = 500$  MeV is given in the lower part where the 'mean-field' contribution only shows up as tiny ridges, that extend up to  $q \simeq 0.3$  GeV/c, i.e. up to the region of the Fermi momentum. Beyond this value the distribution is dominated by the correlations. The dashed line indicates the maximum of the spectral function for high momenta attributed to short-range and tensor correlations as

$$E_R = 2\epsilon + \frac{q^2}{2m_N} \quad (11)$$

with  $\epsilon \simeq 7$  MeV [27]. The simple relation (11) demonstrates that the high internal momenta correspond to high removal energies, too. This is just opposite to the behaviour for momenta below the Fermi level and will be quite important for subthreshold particle production, because the contributions from the high momentum component of the nuclear wave function should be negligible close to the absolute threshold since the available energy (including  $E_R$ ) is below threshold.

The relation between the high momentum and high removal energy was for the first time illustrated by Ciofi degli Atti, Pace and Salme [45] considering the saturation of the momentum sum rule, i.e.

$$\Phi(q) = \int_{E_{th}}^{E_{max}} dE_R S(q, E_R), \quad (12)$$

where  $E_{th}$  is the single nucleon removal threshold. In Fig. 2 we show the function (12) for a  $^{12}\text{C}$  target when integrating up to  $E_{max} = 30, 100, 200$  and  $500$  MeV. It becomes clear that momenta below the Fermi momentum are essentially related to a small removal energy, which is again in reasonable agreement with the mean-field approximation.

The function (12), integrated up to infinity, is the nuclear momentum distribution. Respective momentum distributions for  $^3\text{He}$ ,  $^{12}\text{C}$ , and  $^{208}\text{Pb}$ , that have been calculated with the spectral functions from [27], are shown in Fig. 3. We display separately the

contributions from the uncorrelated part (dashed line) as well as the saturation of the momentum sum rule for the correlated part at  $E_{max}=30$  MeV (dotted line) and 100 MeV (dashed-dotted line). The uncorrelated part of the spectral function includes the ground and one-hole states of the residual nucleus. The short-range and tensor parts of the realistic  $NN$  interactions deplete the states below the Fermi level and partially occupy the states above thus generating the component of  $S(q, E_R)$  with high momentum and high removal energy. The momentum distribution corresponding to the correlated part for  $E_{max} = 30$  MeV (dotted lines) is found to be small for all nuclei in comparison to the 'mean-field' contribution.

### 3.2 Cross sections for pion induced reactions

For our calculations we will need the elementary particle production channels over a wide kinematical regime and, in particular, down to the reaction threshold, where the experimental data often do not exist. In this section we, therefore, formulate a parametrization that allows us to perform an extrapolation of the cross section into the unmeasured region.

The cross sections for meson production from  $\pi + N$  collisions can be separated into two parts. The first one is an exclusive cross section related to binary processes, which are dominant at energies close to the reaction threshold, whereas the second part contains the inclusive production at higher energies.

The cross section for the exclusive  $K^+$  meson production from  $\pi + N$  collisions has been calculated by Tsushima et al. [47]; we adopt their results for our present study.

The cross section for  $\rho$ ,  $\omega$  and  $\phi$ -meson production from the reaction

$$\pi + N \rightarrow R \rightarrow M + N \quad (13)$$

is most conveniently described within a resonance model. Assuming that the squared matrix element is proportional to a Breit-Wigner function the cross section for the reaction (13) can be written as

$$\sigma(\pi + N \rightarrow M + N; s) = \frac{\pi}{k^2} \frac{2J + 1}{2} \frac{B_{in} B_{out} \Gamma^2}{(\sqrt{s} - M_R)^2 + \Gamma^2/4} \times R_2(s), \quad (14)$$

where  $J$ ,  $B_{in}$  and  $B_{out}$  are the resonance spin and the branching ratios of the incoming and outgoing channels respectively, while the factor  $R_2$  stands for the phase-space volume of the final particles,

$$R_2 = \pi \lambda^{1/2}(s, m_N, m_M) / s^{1/2}, \quad (15)$$

with  $m_N$  and  $m_M$  denoting the masses of the nucleon and meson, respectively. In Eq. (14)  $k^2$  is given by

$$k^2 = \lambda(s, m_\pi, m_N) \quad (16)$$

with the Källén function

$$\lambda(z, x, y) = [z - (x + y)^2] [z - (x - y)^2] / 4z. \quad (17)$$

The parameters  $M_R$  and  $\Gamma$  from Eq. (14) are the mass of the 'baryon resonance' and full width, respectively. We note that within the resonance description we neglect coherent contributions from the available baryons as well as possible interference terms since we do not have experimental information on their actual magnitude.

Within our semiphenomenological approach we now fit the experimental data on  $\rho$ ,  $\omega$  and  $\phi$ -meson production in pion induced reactions in order to extract the mass and width of the 'effective' resonance  $R$ . Our fits to the data [48] are shown in Figs. 4,5,6 with the parameters listed in Tab. 1. For convenience, the data are plotted as a function of  $\sqrt{s} - \sqrt{s_{th}}$ , with  $s$  denoting the squared invariant energy of the colliding particles and  $\sqrt{s_{th}} = 2m_N + m_M$  in accordance with the reaction threshold. In Figs. 4,5,6 the fitted resonance cross section for the exclusive reactions  $\pi + N \rightarrow \omega + N$ ,  $\rho + N$ ,  $\phi + N$ , are given by the dashed lines in comparison to the data from [48].

Since there are not enough experimental data available for the inclusive  $\rho$ ,  $\omega$  and  $\phi$ -meson production from  $\pi + N$  collisions that allow to construct reliable parametrizations, we calculate the cross sections for the inclusive meson production within the Lund-String-Model (LSM) from [49]. The calculated results within the Lund-String-Model can be fitted by a function of the form

$$\sigma(\pi + p \rightarrow M + X) = a(x - 1)^b x^{-c} \quad (18)$$

from threshold up to a few 100 GeV, where the scaling variable is defined as

$$x = s/s_{th}. \quad (19)$$

The parameters for all interesting channels  $a$ ,  $b$ ,  $c$  and  $s_{th}$  are listed in Tab. 2.

Our fits to the LSM results are shown by the solid lines in Figs. 4,5,6 and reasonably well reproduce the available inclusive data on vector meson production from inclusive processes at high energies. For practical purposes we will use the maximum of the 'resonance' cross section (14) and the LSM parametrization (18) for the inclusive vector meson cross sections.

The Lorentz invariant differential cross sections entering Eqs. (1) and (5), finally, due to two-body kinematics near threshold are completely determined when assuming an isotropic distribution in the pion-nucleon cms.

### 3.3 Proton induced reactions.

The cross sections for  $K^+$ ,  $\rho$ ,  $\omega$  and  $\phi$ -meson production from  $p + p$  collisions within the Lund-String-Model (LSM) are shown in Figs. 7,8,9,10 as a function of the invariant collision energy  $\sqrt{s}$  in comparison to the experimental data from [48]. The solid lines show the fit to the LSM results according to Eq. (18) with the parameters from Tab. 3, whereas in case of  $\omega$  production the full dots stand for the LSM results. We additionally show the cross sections for exclusive meson production within the One-Boson Exchange Model (OBEM) [50] by the dashed lines in comparison to the respective data from [48] (triangles). Whereas in case of  $K^+$ ,  $\rho$ ,  $\omega$  production the inclusive LSM results smoothly match with the OBEM calculations for the exclusive channels close to threshold, this is no longer the case for  $\phi$ -meson production (cf. Fig. 10) because the string fragmentation model requires the formation of two  $s\bar{s}$ -pairs, which shifts the threshold up to higher

energies. Since there are presently no experimental data available for  $\sqrt{s} < 3.5$  GeV in case of  $p + p$  reactions we will adopt the maximum of the cross sections from the OBEM and LSM calculations for the inclusive  $\phi$ -meson production as in the case of the  $\pi + N$  reactions.

Though our present results for the  $p + N$  channels have some uncertainty close to threshold, this will not show up sensitively in  $p + A$  reactions since the pion induced channels contribute more effectively (cf. Section 4).

### 3.4 The effective collision number

The factor  $N_{eff}(E)$  appearing in Eqs. (1), (5) accounts for the  $A$ -dependence of the  $K^+$ ,  $\rho$ ,  $\omega$  and  $\phi$ -meson production as well as for the Final State Interaction (FSI) of the mesons in the nuclear medium. As first proposed by Margolis [51], the  $A$ -dependence for particle production and propagation in the nuclear medium can be described by extending the Glauber multiple scattering theory [52]. In accordance with [53, 54] this gives

$$N_{eff} = \int_0^{+\infty} b db \int_{-\infty}^{+\infty} \rho(b, z) dz \int_0^{2\pi} d\phi \times \left[ \exp\left(-\sigma_{pN} \int_{-\infty}^z \rho(b, \xi) d\xi - \sigma_{MN} \int_0^{+\infty} \rho(\mathbf{r}[\zeta]) d\zeta\right) \right], \quad (20)$$

where  $\rho(\mathbf{r})$  is the single-particle density in coordinate space (taken from [55]) normalized to the target mass number. Here,  $\mathbf{r}[\zeta]$  is

$$\mathbf{r}[\zeta] = \mathbf{r}_0(b, 0, z) + \zeta \hat{\mathbf{e}}, \quad (21)$$

where  $b$  and  $z$  stand for the impact parameter and the  $z$ -component of the coordinate along the beam-axis, respectively, and  $\hat{\mathbf{e}}$  is a unit vector in coordinate space in the form

$$\hat{\mathbf{e}} := (\sin\theta\cos\phi, \sin\theta\sin\phi, \cos\theta), \quad (22)$$

while  $\theta$  is the meson emission angle in the laboratory system. Moreover,  $\sigma_{pN}$  is the total  $p + N$  cross section while  $\sigma_{MN}$  is the  $M + N$  absorption cross section.

Within the small angle approximation, i.e. for  $\theta \simeq 0^\circ$ , one can reduce (20) to

$$N_{eff} = \frac{1}{\sigma_{pN} - \sigma_{MN}} \int d^2b \left( \exp[-\sigma_{MN} T_A(b)] - \exp[-\sigma_{pN} T_A(b)] \right) \quad (23)$$

with  $T_A(b)$  denoting the profile function of the target [52]. In Eq. (23) the second term is related to the effective number of nucleons (of the target) participating in the interaction with the impinging proton while the first term accounts for the final state reabsorption.

As shown in [17, 38]  $N_{eff}$  from Eq. (23) for  $\sigma_{MN} \simeq 0$  can adequately be parameterized by

$$N_{eff} = A^{0.75 \pm 0.01}, \quad (24)$$

at bombarding energies above 0.8 GeV, where  $A$  is again the target mass number. Thus the  $A$ -dependence of the direct production mechanism is proportional to (24)



whenever the produced meson only weakly interacts with the residual nucleus. In case of  $\sigma_{pN} \gg \sigma_{MN}$  we can - assuming a uniform distribution of the nuclear density - reduce the absorption term from (23) to the simple expression

$$\kappa = \exp[-\sigma_{MN}\rho_0 R_A], \quad (25)$$

where  $\rho_0 = 0.168 \text{ fm}^{-3}$  and  $R_A$  are the average density and the radius of the nucleus, respectively. We note that the factor  $\kappa$  is frequently used to describe the reabsorption of the produced particles in finite nuclei in order to account for weak reabsorption effects.

However, the application of (25) in case of  $\rho$  and  $\omega$  production is not adequate because the reabsorption cross section  $\sigma_{MN}$  appearing in (20-25) is no longer small compared to  $\sigma_{pN}$ . In order to demonstrate the sensitivity of  $N_{eff}$  to the various approximation schemes (20), (23), (25) we show in Fig.11 the effective collision number for  $^{12}\text{C}$  as a function of the reabsorption cross section within the limits of Eq. (20) (solid line), Eq. (23) (dashed line) and Eq. (25) (dotted line) which deviate substantially already for absorption cross sections of about 30 mb. Consequently, we will use Eq. (20) in the following to describe the inclusive production and absorption of mesons in  $p + A$  reactions with the absorption cross sections described in Section 3.5

We, furthermore, note that by Eq. (20) we only account for reabsorption and neglect elastic meson-nucleon rescattering. This is of no special interest when considering inclusive (integrated) cross sections only as in Section 4, but will be essential when comparing the Lorentz invariant spectra with experimental data sets in a narrow kinematic regime. For the latter purpose transport simulations as described in ref. [56] will provide a more adequate description.

The calculation of  $N_{eff}$  for the two-step reactions with an intermediate pion has been described by Vercellin et al. [54] within the Glauber formalism and is a more involved task. However, as shown in [38], a practicable approximation is to use  $N_{eff}$  from Eq. (20) and to include the corrections from the two-step mechanism by a factor  $g_\pi$  as

$$g_\pi = 1 - \frac{1}{4R_A^2} \left( \frac{1}{\sigma_{pN}\rho_0} + \frac{1}{\sigma_{\pi N}\rho_0} \right)^2, \quad (26)$$

which describes the average probability for a pion to scatter again in the target with radius  $R_A$ . In case of small final meson ( $K^+$ ,  $\rho$ ,  $\omega$ ,  $\phi$ ) reabsorption the  $A$ -dependence of the inclusive production cross section due to the reactions with an intermediate pion roughly scales as

$$N_{eff} \times g_\pi \simeq A^{1.2 \pm 0.1}. \quad (27)$$

### 3.5 $\rho, \omega, \phi$ -nucleon cross sections

The total cross sections for  $V+N$  interactions at high energies can be evaluated with the Vector-meson Dominance Model (VDM) from  $\rho$ ,  $\omega$  and  $\phi$ -meson photoproduction [57] or be obtained within the additive quark model relations [58, 59] from measurable cross sections. The results obtained with the VDM [60] are in good agreement with those computed via quark sum rules, resulting in  $\sigma_{\rho N} = \sigma_{\omega N} \simeq 25 \text{ mb}$  and  $\sigma_{\phi N} \simeq 12 \text{ mb}$  at vector meson momenta above 1 GeV/c.

The cross sections for  $\rho + N$ ,  $\omega + N$  and  $\phi + N$  interactions in case of low relative momenta can be extracted from the  $\pi + N$  reactions by assuming that this is the dominant absorption channel. Detailed balance provides the relation

$$\frac{\sigma_{\pi+N \rightarrow M+N}}{\sigma_{M+N \rightarrow \pi+N}} = \frac{(2I_N + 1)(2I_M + 1) \lambda(s, m_N, m_M)}{(2I_\pi + 1)(2I_N + 1) \lambda(s, m_N, m_\pi)}, \quad (28)$$

where  $s$  is the squared invariant energy,  $m_N$ ,  $m_\pi$ ,  $m_M$  are the masses, while  $I_N$ ,  $I_\pi$  and  $I_M$  are the spins of nucleon, pion and vector meson, respectively. Here, the function  $\lambda$  is given by (17). With our parametrizations for the cross sections  $\sigma_{\pi+N \rightarrow M+N}$  (14) we then obtain the cross sections for vector meson-nucleon interactions via (28).

The cross sections extracted from detailed balance are only related to the particular inelastic reaction channel  $MN \rightarrow \pi N$ , and do not saturate the total cross sections even at momenta of 100 MeV/c. Indeed the  $2\pi N$ ,  $3\pi N$ ,  $m\pi N$  or  $K\bar{K}N$  final states as well as elastic scattering can also occur, which all contribute to the total cross sections. Since there are no reliable calculations on the  $V + N$  cross sections at low energy [61], we adopt the results from the VDM.

## 4 Results for $p + {}^{12}\text{C}$

After specifying all the elementary cross sections in proton and pion induced channels as well as the spectral function  $S(q, E_R)$  [27, 46] we now present the results for meson production cross sections in  $p + {}^{12}\text{C}$  collisions according to (1) and (5). Though our primary interest are the vector mesons, we first discuss our calculations for  $K^+$  production in comparison to the data from Koptev et al. [19] and the results from the folding model [13]. In Fig. 12 we thus compare the cross sections within the spectral function approach for the one-step channel (dashed line) and the two-step mechanism (solid line) with the one-step (dash dotted line) and two-step result (dotted line) from the folding model with elementary cross sections as described in ref. [38].

Note that the folding model, contrary to the spectral function approach, is a pure mean-field approximation, where the nucleon momentum distribution for the target nucleus is calculated in the Hartree-Fock limit [38] corresponding to the dashed line in Fig. 3. Thus the high momentum components, that are associated with the correlated part of the spectral function (cf. Fig. 3), are missing in the folding model calculations [38]. The dispersion relation for a target nucleon in the folding model was taken as

$$\omega(q) = \sqrt{q^2 + m_N^2} - \epsilon \quad (29)$$

where  $\epsilon$  is again the average binding energy per nucleon. In spite of the quite different assumptions in both approaches, the results for the  $K^+$ -meson cross sections for one-step and two-step reaction channels are remarkably close to each other.

Whereas at energies above 0.95 GeV both results are practically the same, the folding model with the quasi-free dispersion relation (29) for the target nucleon overestimates the energy available in the collision and thus leads to slightly higher cross sections than our spectral function approach for both reaction steps at lower bombardment energy. Thus the underestimation of the data below about  $T_0 = 0.92$  GeV might

be considered as an evidence for additional many-body effects or further production channels that become important close to the reaction threshold. On the other hand, the dominance of the two-step reaction mechanism is the same within both approaches and can be considered as model independent.

Since in the spectral function from [46] we cannot separate the correlated and uncorrelated parts, we adopt the spectral function from [27], that allows the separation of the two components. Within the latter parametrization we can study the relative contribution from the correlated part of  $S_P(q, w)$  for meson production in  $p + A$  reactions. Our calculated results for  $K^+$ -meson production in  $p + {}^{12}\text{C}$  collisions are shown in Fig. 13 for the two-step mechanism (solid line) and primary reaction channel (dashed line) in comparison with the experimental data [19]. In line with our arguments presented above the contributions from the correlated part of the spectral function indeed are small compared to the data.

For more pedagogical reason we also discuss the results for the  $K^+$ -meson production cross section when employing the momentum distribution  $\Phi(q)$ , as obtained from integrating the spectral function from [27] over the removal energy, but using the free dispersion relation

$$\omega = \sqrt{m_N^2 + \mathbf{q}^2}, \quad (30)$$

for all momenta with  $m_N$  being the mass of free nucleon and  $\mathbf{q}$  the nuclear momentum taken in accordance with the function  $\Phi(q)$  from [27] shown in Fig. 3.

In this unrealistic limit the one-step production mechanism (dashed-dotted line in Fig. 13) still underestimates the experimental data by more than a factor of 5, however, the results for the two-step mechanism now overestimates the data by almost an order of magnitude. This comparison clearly demonstrates that the high momentum component appearing in the spectral function approach cannot be exploited in a quasi-free production mechanism.

We continue with our calculations for the vector mesons in  $p + {}^{12}\text{C}$  reactions. The results are shown in Fig. 14; here, the solid lines indicate the contribution from the two-step reactions with an intermediate pion (5), while the dashed lines correspond to the direct production mechanism (1) using again the spectral function from [46]. For all mesons ( $\rho$ ,  $\omega$ ,  $\phi$ ) the two-step mechanism is clearly dominant close to threshold and kinematically is due to the effect that the Fermi motion of the nucleons is exploited twice in the two-step channels. The absolute cross sections at about 2 GeV are in the order of 10  $\mu\text{b}$  for  $\rho$ ,  $\omega$ -production, which is high enough to allow for a detailed experimental study at COSY or CELSIUS.

## 5 Summary

In this work we have presented an approach for meson production in  $p + A$  reactions on the basis of direct and two-step production channels (including an intermediate pion) on the basis of the nuclear spectral function without incorporating any selfenergies for the mesons. The 'elementary' cross sections for  $\rho, \omega$  and  $\phi$  production have been evaluated within the LUND string formation and fragmentation model [49] and within a resonance model for  $\pi N$  collisions close to threshold, respectively. The available

experimental data from [48] for the exclusive and inclusive reactions are described sufficiently well, however, our extrapolations for the various channels close to threshold should be controlled experimentally in the near future.

Whereas in previous reaction models only the target momentum distribution has been employed using a quasi-free dispersion relation for the target nucleons, our present formulation is based on the full spectral function  $S(q, \omega)$  where the nucleon may be far off-shell and high momentum, high removal energy components appear as well.

This approach was first used by Debowski, Grosse and Senger [23, 24] for proton induced particle production. While those authors applied the method to their own measured differential spectra for  $K^+$ -meson production on  $^{12}C$  and  $^{208}Pb$ , we have tested our approach for  $K^+$  production in comparison to the experimental data from Koptev et al. [19] using the spectral function for  $^{12}C$  from ref. [46].

What emerges from a detailed study of the spectral function is that one should use a quasifree dispersion relation (10) only for nuclear momenta below the Fermi level. For higher values of  $q$  a dispersion relation with (11) should be used for the origin of the high momentum component accounting for two-body correlations.

It is clearly seen that the two-step mechanism with an intermediate pion gives by far the dominant contribution at subthreshold energies as in the folding model [13], but the actual cross section for  $K^+$ -meson is underestimated below about 920 MeV indicating the need for further reaction channels or many-body effects. This result contrasts with the folding model where a better description of the data is achieved. We attribute this to the fact that the folding model - adopting a quasi-free dispersion relation for the target nucleon - overestimates the available energy in nucleon-nucleon collisions when approaching the absolute reaction threshold.

On the other hand, when integrating the spectral function over the energy  $E_R$ , we obtain a momentum distribution showing very high momentum components that can be attributed to short-range nucleon-nucleon or tensor correlations. However, these high momentum components on average are associated with high removal energies, too, such that they cannot be exploited for meson production close to the absolute reaction threshold. Thus, meson production close to threshold does not provide information on the high momentum components in finite nuclei or short-range two-body correlations.

Within our approach we have also calculated the cross sections for the vector mesons  $\rho$ ,  $\omega$ ,  $\phi$  in  $p + ^{12}C$  collisions from threshold up to a few GeV. We obtain estimates for their production in nuclei without incorporating any selfenergies for the mesons. These cross sections provide a baseline for experiments at COSY or CELSIUS that address the in-medium properties of the vector mesons as well as their final state interaction with nuclei. Here, in context with chiral symmetry restoration, the  $\rho$  and  $\omega$ -mass at normal nuclear density  $\rho_0$  is expected to be reduced by about 18% [8], which will sizeably enhance their production cross section as compared to our calculations for free vector mesons presented above. A detailed study of their production cross section as a function of  $T_0$  and target mass  $A$  might help to separate the effects from the real and imaginary part of the meson selfenergies.

The authors acknowledge many fruitful discussions with M. Büscher, E. Grosse and B. Kamys. They like to thank, furthermore, I. Sick for providing the  $^{12}\text{C}$  spectral function in numerical form.

## References

- [1] Grimm, P., Grosse, E.: Prog. Part. Nucl. Phys. **15**, 339 (1985)
- [2] Braun-Munzinger, P. Stachel, J.: Ann. Rev. Nucl. Part. Sci. **37**, 1 (1987)
- [3] Mosel, U.: Ann. Rev. Nucl. Part. Sci. **41**, 29 (1991)
- [4] Jakobsson, B.: Phys. Scripta **48**, 179 (1993)
- [5] Shyam, R., Knoll, J.: Nucl. Phys. A **483**, 711 (1988)
- [6] Bertsch, G.F., Das Gupta, S.: Phys. Rep. **160**, 189 (1988)
- [7] Cassing, W., Metag, V., Mosel, U., Niita, K.: Phys. Rep. **188**, 363 (1990)
- [8] Hatsuda, T, Lee, S.: Phys. Rev. C **46**, R34 (1992)
- [9] Agakichiev, G., Baur, R., Breskin, A., Chechnik, R., Drees, A., et al., Phys. Rev. Lett. **75**, 1272 (1995)
- [10] Masera, M., et al.: Nucl. Phys. A **590**, 93c (1995)
- [11] Cassing, W., Eehalt, W., Ko, C.M.: Phys. Lett. B **363**, 35 (1995); Cassing, W., Eehalt, W., Kralik, I.: Phys. Lett. B **377**, 5 (1996)
- [12] Li, G.Q., Ko, C.M., Brown, G.E.: Phys. Rev. Lett. **75**, 4007 (1995)
- [13] Cassing, W., Batko, G., Vetter, T., Wolf, G.: Z. Phys. A **340**, 51 (1991)
- [14] Cugnon, J., Lombard, R.M.: Nucl. Phys. A **422**, 635 (1984)
- [15] Golubeva, E.S., Ilinov, A.S., Pshenichnov, I.A.: Nucl. Phys. A **562**, 389 (1993)
- [16] Müller, H., Sistemich, K.: Z. Phys. A **344**, 197 (1992)
- [17] Sibirtsev, A., Büscher, M.: Z. Phys A **347**, 191 (1994)
- [18] Sibirtsev, A.A.: Sov. J. Nucl. Phys. **55**, 729 (1992)
- [19] Koptev, V.P., Mikirtyhyants, S.M., Nesterov, M.M., Tarasov, N.A., Scherbakov, G.V., et al.: JETP **94**, 1 (1988)
- [20] Chiavassa, E., Dellacassa, G., De Marco, N., Ferrero, F., Gallio, M., et al.: Z. Phys. A **344**, 345 (1993)
- [21] Chiavassa, E., Dellacassa, G., De Marco, N., Ferrero, F., Musso, M., et al.: Z. Phys. A **342**, 107 (1992)

- [22] Chiavassa, E., Dellacassa, G., De Marco, N., Ferrero, F., Gallio, M., et al.: Nucl. Phys. A **538**, 121 (1992)
- [23] Debowski, M., Grosse, E., Senger, P.: Preprint GSI **10-95**, 3 (1995)
- [24] Debowski, M.: Ph.D. Thesis (1995)
- [25] Sibirtsev, A., Büscher, M., Müller, H., Schneiderei, Ch.: Z. Phys. A **351**, 333 (1995)
- [26] Day, D., McCarthy, J.S., Meziani, Z.E., Minehart, R., Sealock, R., et al.: Phys. Rev. C **48**, 1849 (1993)
- [27] Ciofi degli Atti, C., Simula, S.: Phys. Rev. C **53**, 1689 (1996)
- [28] Kerman, A.K., Manus, H.Mc, Thaler, R.M.: Annals of Phys. **8**, 55 (1959)
- [29] Newton, R.G.: Scattering Theory of Waves and Particles, New York, McCraw-Hill (1966).
- [30] Jackson, D.F.: Nuclear Reactions, London, Methuen (1970).
- [31] Satchler, G.R.: Introduction to Nuclear Reactions, Hong Kong, Macmillan Education LTD (1990)
- [32] Weber, K., Blättel, B., Cassing, W., Dönges, H.-C., Koch, V., Lang, A., Mosel, U.: Nucl. Phys. A **539**, 713 (1992)
- [33] Cooper, E.D.: Phys. Rev. C **36**, 2170 (1987)
- [34] Hama, S., Clark, B.C., Cooper, E.D., Sherif, H.S., Mercer, R.L.: Phys. Rev. C **41**, 2737 (1990)
- [35] Welke, G.M., Prakash, M., Kuo, T.T.S., Das Gupta, S., Gale, C.: Phys. Rev. C **38**, 2101 (1988)
- [36] Sibirtsev, A.A.: Phys. Scr. RS **21**, 167 (1993)
- [37] Kilian, K., Nann, H.: Meson production near threshold, ed. H. Nann and E.J. Stephenson, AIP Conf. Proc. **221**, 185 (1990)
- [38] Cassing, W., Batko, G., Mosel, U., Niita, K., Schult, O., Wolf, Gy.: Phys. Lett. B **238**, 25 (1990)
- [39] Cugnon, J., Lemaire, M.-C.: Nucl. Phys. A **489**, 781 (1988)
- [40] Sibirtsev, A., Tsushima, K., Faessler, A.: Z. Phys. A **354**, 215 (1996)
- [41] Guet, C., Prakash, M.: Nucl. Phys. A **428**, 119 (1984)
- [42] Frullani, S., Mougey, J.: Adv. Nucl. Phys. **14**, 7 (1984)

- [43] Benhar, O., Fabrocini, A., Fantoni, S.: Nucl. Phys. A **505**, 267 (1989)
- [44] Mahaux, C., Sartor, R.: Nucl. Phys. A **546**, 65 (1992)
- [45] Ciofi degli Atti, C., Pace, E., Salme, G.: Phys. Rev. C **21**, 805 (1980)
- [46] Sick, I., Fantoni, S., Fabrocini, A., Benhar, O.: Phys. Lett. B **323**, 267 (1994) and private communication.
- [47] Tsushima, K., Huang, S.W., Faessler, A.: Phys. Lett. B **337**, 245 (1994)
- [48] Landolt-Börnstein, New Series, ed H. Schopper, **I/12** (1988)
- [49] Nilsson-Almqvist, B., Stenlund, E.: Comp. Phys. Comm. **43**, 387 (1987)
- [50] Sibirtsev, A.A.: to be pub. in Nucl. Phys. A.
- [51] Margolis, B.: Phys. Lett. B **26**, 524 (1968)
- [52] Glauber, R.J., Mathiae, J.: Nucl. Phys., B **21**, 135 (1970)
- [53] Margolis, B.: Nucl. Phys. B **4**, 433 (1968)
- [54] Vercellin, E., Chiavassa, E., Dellacasa, G., et al.: Nuovo Cimento A **106**, 861 (1993)
- [55] Knoll, J., Randrup, J.: Nucl. Phys. A **324**, 445 (1979)
- [56] Rudy, Z., Cassing, W., Demski, T., Jarczyk, L., Kamys, B., et al.: Z. Phys. A **351**, 217 (1995)
- [57] Sakurai, J.J.: Ann. Phys. (NY) **11**, 1 (1960)
- [58] Joos, H.: Phys. Lett. B **24**, 103 (1967)
- [59] Kajantie, K., Trefil, J.S.: Phys. Lett. B **24**, 106 (1967)
- [60] Christillin, P.: Phys. Rep. **190**, 64 (1990)
- [61] Sibirtsev, A., Dolgolenko, A.G.: to be pub. in Sov. J. Nucl. Phys. (1996)

Table 1: The effective mass and width of the baryonic resonance in Eq. (14), as well as  $B = B_{in} \times B_{out} \times (2J + 1)$ .

Meson	$M_R$ (GeV)	$\Gamma$ (GeV)	$B$ ( $\mu\text{bGeV}^{-2}$ )
$\rho^0$	1.809	0.99	413
$\omega$	1.809	0.99	302
$\phi$	1.8	0.99	5.88

Table 2: The parameters of Eq. (18) for pion induced reactions. Here the index <sup>(1)</sup> implies a shift  $x \rightarrow x - 1.3$ .

Meson	$s_{th}$ ( $\text{GeV}^2$ )	$a$ (mb)	$b$	$c$
$\rho^0$	2.917	3.6	1.47	1.25
$\omega$	2.958	4.8	1.47	1.26
$\phi^{(1)}$	3.831	0.09	2.54	2.1

Table 3: The parameters of Eq. (18) for proton induced reactions. Here the index <sup>(1)</sup> implies a shift  $x \rightarrow x - 1.3$ .

Meson	$s_{th}$ ( $\text{GeV}^2$ )	$a$ (mb)	$b$	$c$
$K^+$	6.49	1.12	1.47	1.22
$\rho^0$	7.01	2.2	1.47	1.1
$\omega$	7.06	2.5	1.47	1.11
$\phi^{(1)}$	8.38	0.09	2.54	2.09
$\eta$	5.88	2.5	1.47	1.25



Figure 1: The spectral function  $S(q, E_R)$  for  $^{12}\text{C}$  from [46]. The dashed line shows the relation (11). The contour lines decrease by a factor of 1.5 from line to line.

Figure 2: Saturation of the momentum sum rule for  $^{12}\text{C}$ . The lines indicate the function (12) integrated up to energy  $E_{max}=30$  MeV (dashed), 100 MeV (dotted), 200 MeV (dash-dotted) and 500 MeV (solid line). The arrow indicates the Fermi momentum.

Figure 3: The momentum distribution for  $^3\text{He}$ ,  $^{12}\text{C}$ , and  $^{208}\text{Pb}$  according to [27]. The dashed lines result from the uncorrelated part of the spectral function. The dotted lines indicate (12) for the correlated spectral function integrated up to  $E_{max} = 30$  MeV and the dashed-dotted lines up to  $E_{max} = 100$  MeV. The solid lines display the sum of the uncorrelated and correlated parts for  $E_{max} \rightarrow \infty$ .

Figure 4: Experimental cross sections for the exclusive reaction  $\pi^+ + p \rightarrow \rho^+ + p$  (triangles) and the inclusive reaction  $\pi^+ + p \rightarrow \rho^0 + X$  (full dots) from [48]. The lines represent our parametrizations as discussed in the text.

Figure 5: Experimental cross sections for the exclusive reactions  $\pi^+ + n \rightarrow \omega + p$  (squares) and  $\pi^- + p \rightarrow \omega + n$  (triangles) and the inclusive reaction  $\pi^+ + p \rightarrow \omega + X$  (full dots). Experimental data are taken from [48]. The lines represent our parametrizations as discussed in the text.

Figure 6: Experimental cross sections for the exclusive reactions  $\pi^+ + n \rightarrow \phi + p$  (squares) and  $\pi^- + p \rightarrow \phi + n$  (triangles) and inclusive reaction  $\pi^+ + p \rightarrow \phi + X$  (dots) from [48]. The lines represent our parametrizations as discussed in the text.

Figure 7: Cross sections for the exclusive reaction  $p + p \rightarrow K^+ + \Lambda + p$  (triangles) and the inclusive reaction  $p + p \rightarrow K^+ + X$  (dots) from [48]. The solid line shows the calculation within the LSM, while the dashed line refers to the OBEM.

Figure 8: Cross sections for the exclusive reaction  $p + p \rightarrow \rho^0 + p + p$  (triangles) and the inclusive reaction  $p + p \rightarrow \rho^0 + X$  (dots) from [48]. The solid line shows the calculation within the LSM, while the dashed line refers to the OBEM.

Figure 9: Experimental cross sections for the exclusive reaction  $p + p \rightarrow \omega + p + p$  (triangles) from [48] in comparison to the OBEM calculation (dashed line). The full dots represent the results from LSM for the inclusive reaction  $p + p \rightarrow \omega + X$ , while the solid line shows our fit with Eq. 16.

Figure 10: Cross sections for the exclusive reaction  $p + p \rightarrow \phi + p + p$  (triangles) and the inclusive reaction  $p + p \rightarrow \phi + X$  (dots) from [48]. The solid line shows the calculation within the LSM and the dashed line our results within the OBEM for the exclusive channel.

Figure 11: The effective collision number calculated with (20)-solid, (23)-dashed and with (25)-dotted line as a function of the meson absorption cross section  $\sigma$  in mb.

Figure 12: Cross section of  $K^+$ -meson production for  $p + {}^{12}C$  as a function of the beam energy  $T_0$ . The solid and dashed lines show the calculations with the total spectral function for the two-step and direct reaction mechanism, respectively, employing the spectral function from [46]. The dotted and dashed-dotted lines show the calculations with mean-field approach (dashed curve in Fig. 3) for the two-step and direct reaction mechanism, respectively, employing a quasifree dispersion relation. The dots show the experimental data from [19]. The solid and the dotted lines were calculated with the same elementary cross sections.

Figure 13: Cross section of  $K^+$ -meson production for  $p + {}^{12}C$  as a function of the beam energy  $T_0$ . The solid and dashed lines are results using only the correlated part of the spectral function from [27] for the two-step and direct reaction mechanism, respectively. The dotted and dashed-dotted lines show the on-shell calculations for the two-step and direct reaction mechanism, respectively. Experimental data are from [19].

Figure 14: Cross section for  $\rho$ ,  $\omega$  and  $\phi$ -meson production in  $p + {}^{12}C$  reactions as a function of the beam energy  $T_0$ . The solid and dashed lines show the calculations with the total spectral function [46] for the two-step and direct reaction mechanism, respectively.

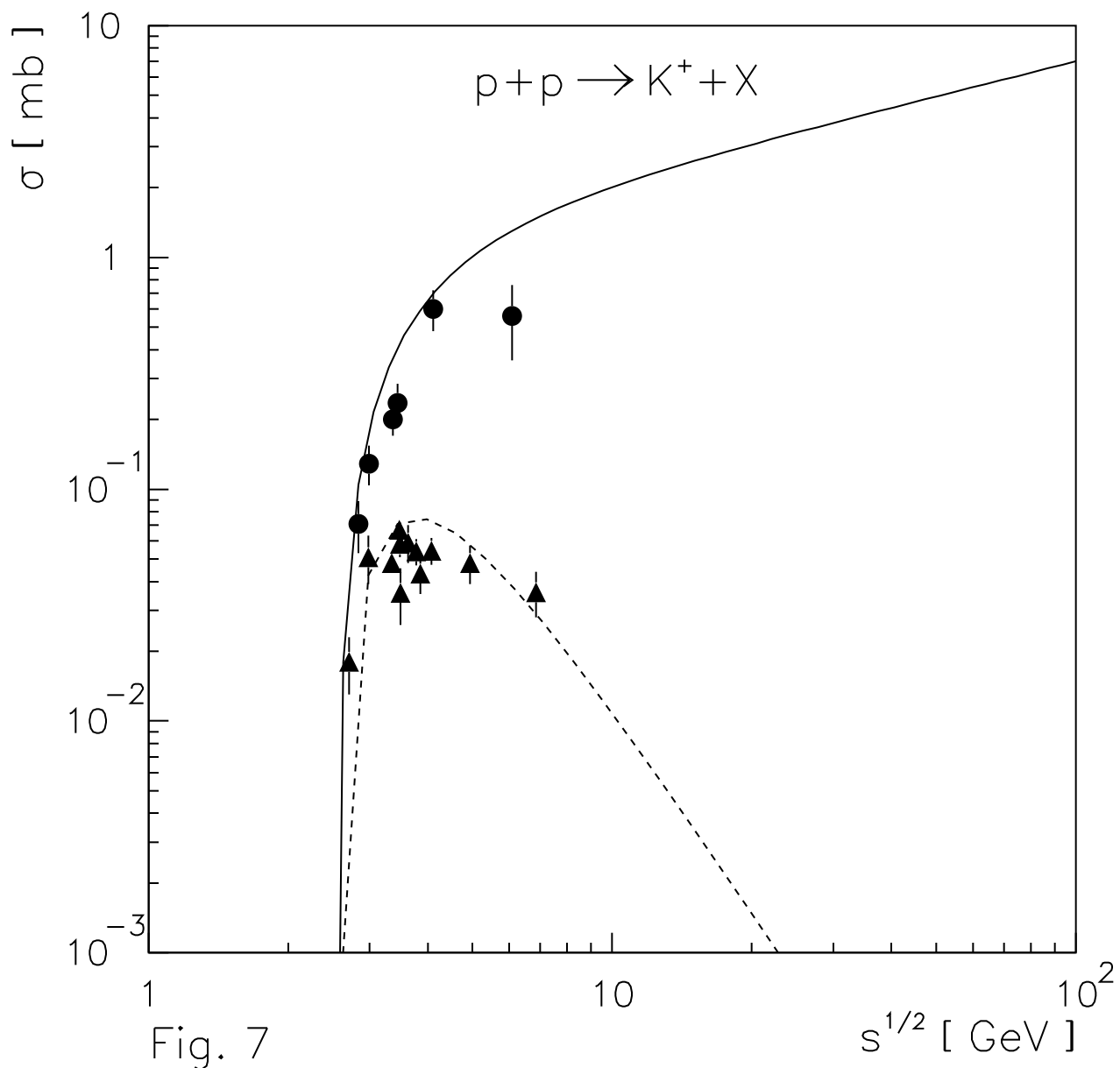


Fig. 7

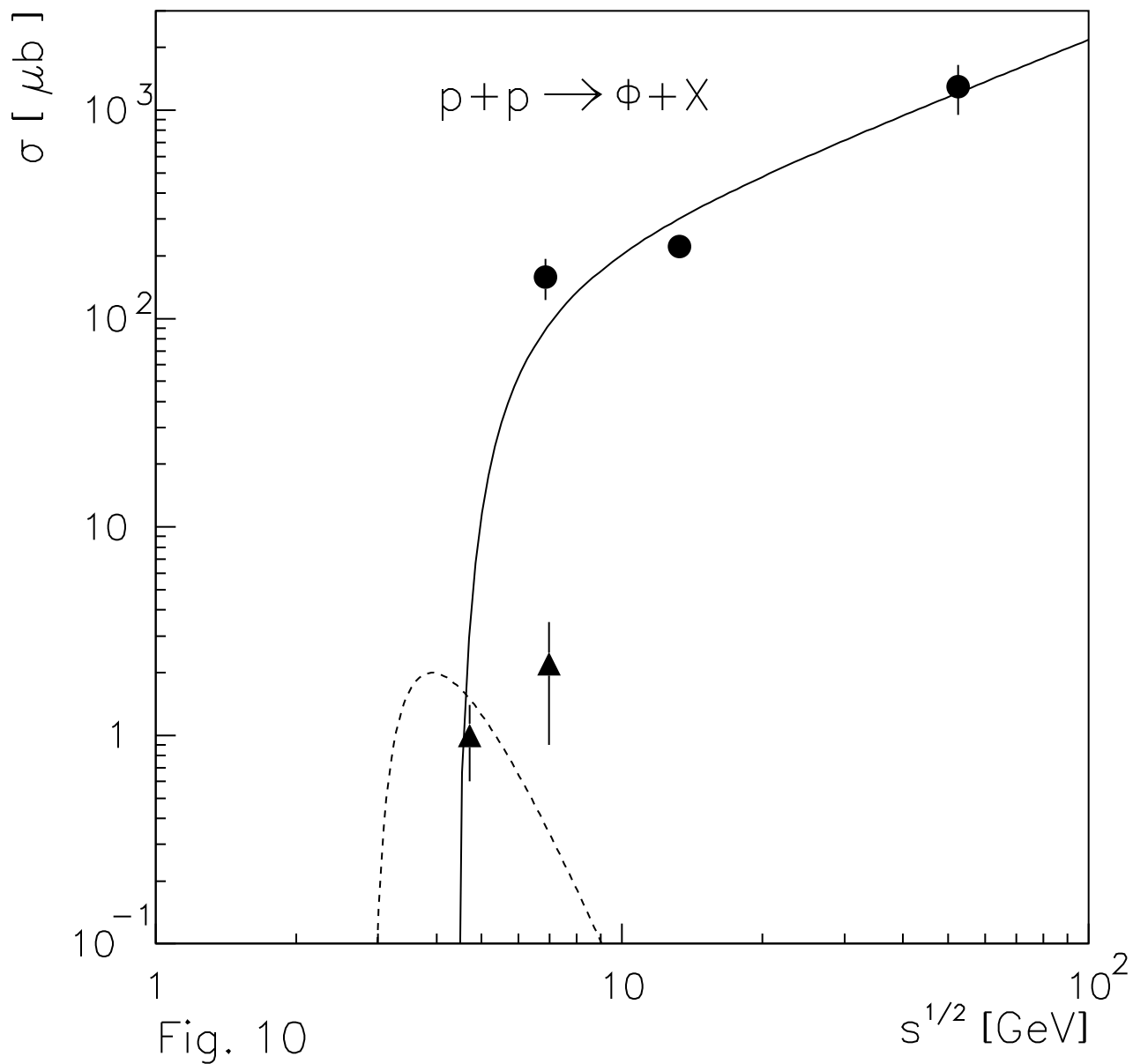


Fig. 10

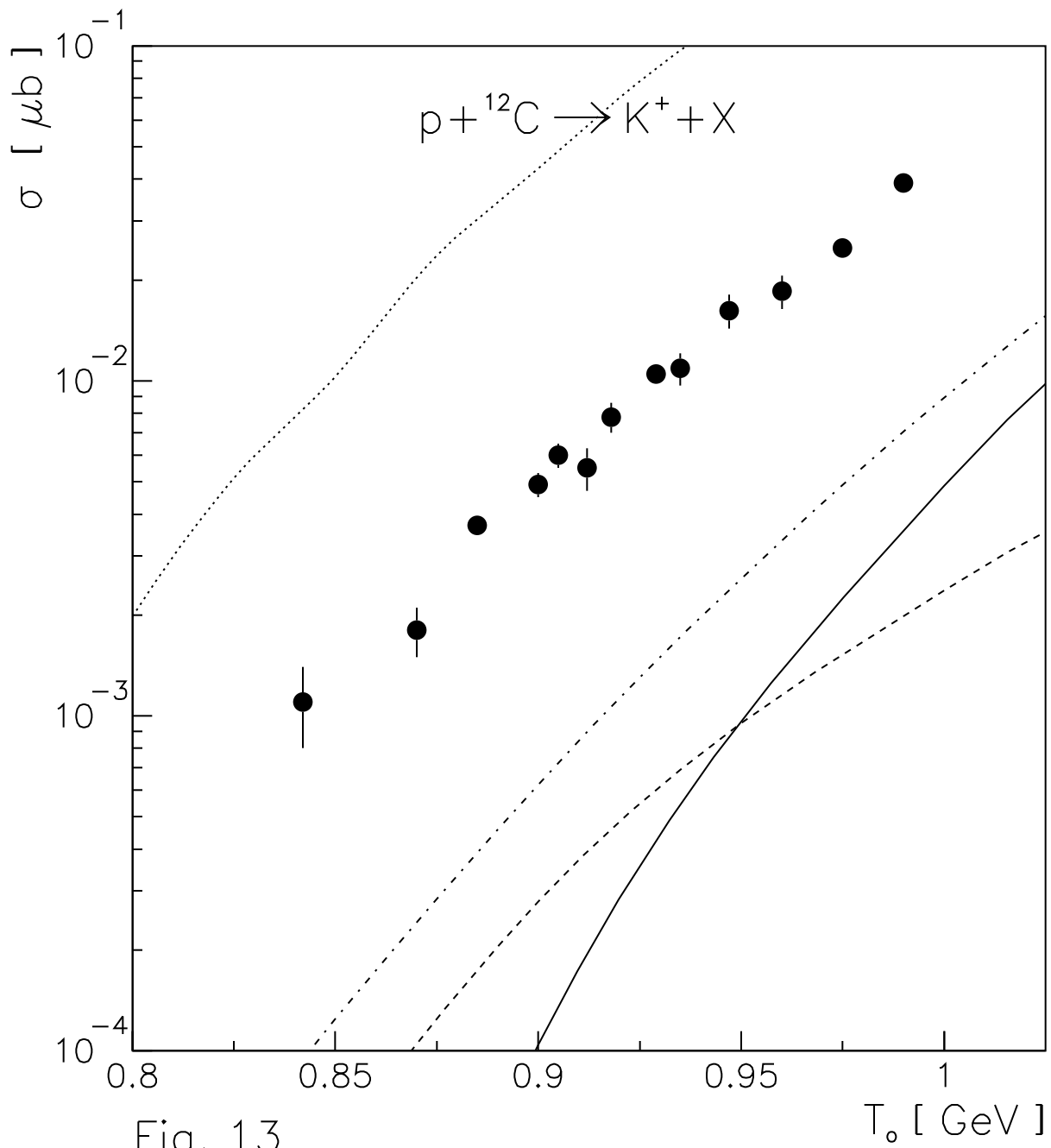


Fig. 13

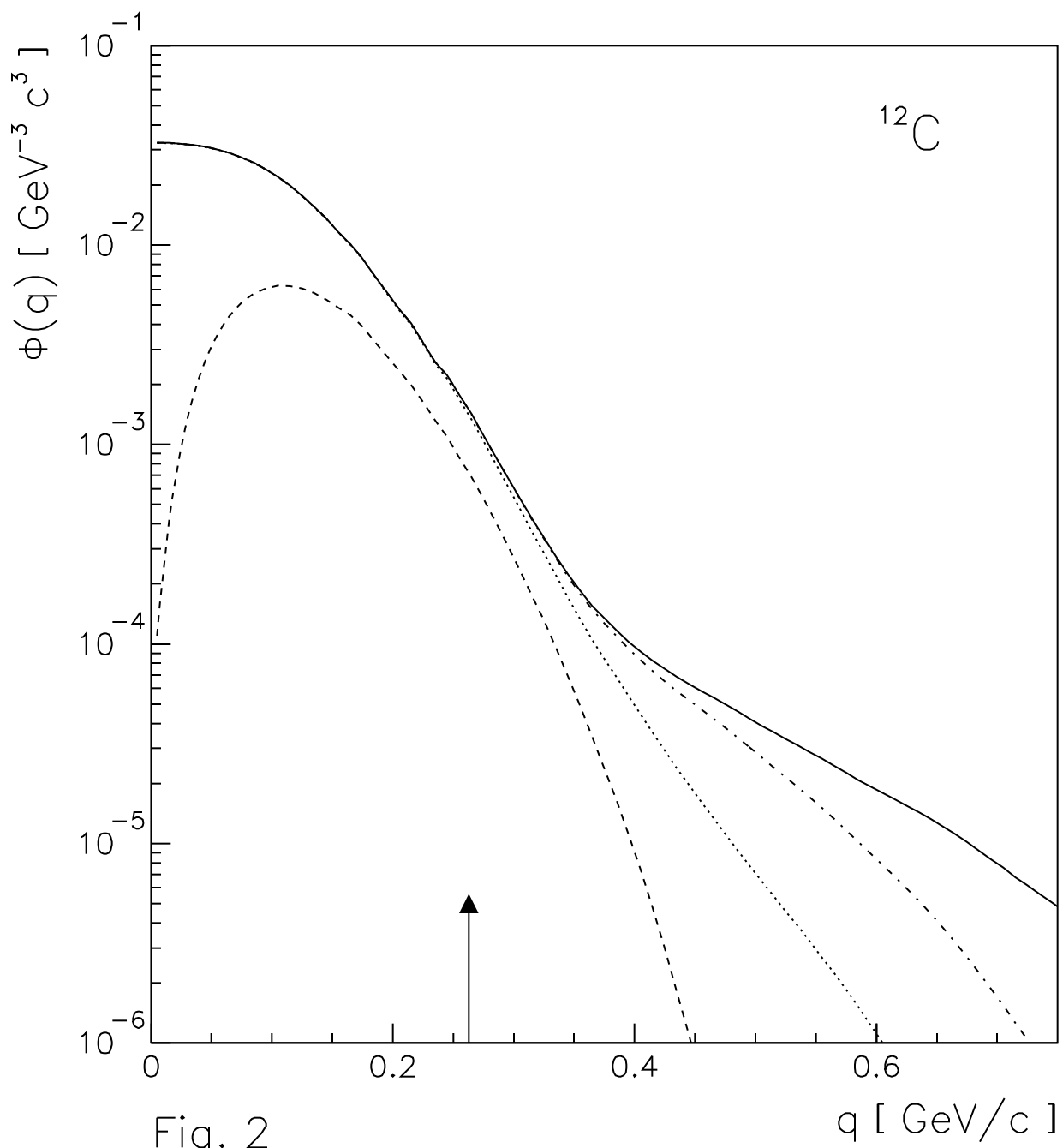


Fig. 2

$q$  [ GeV/c ]

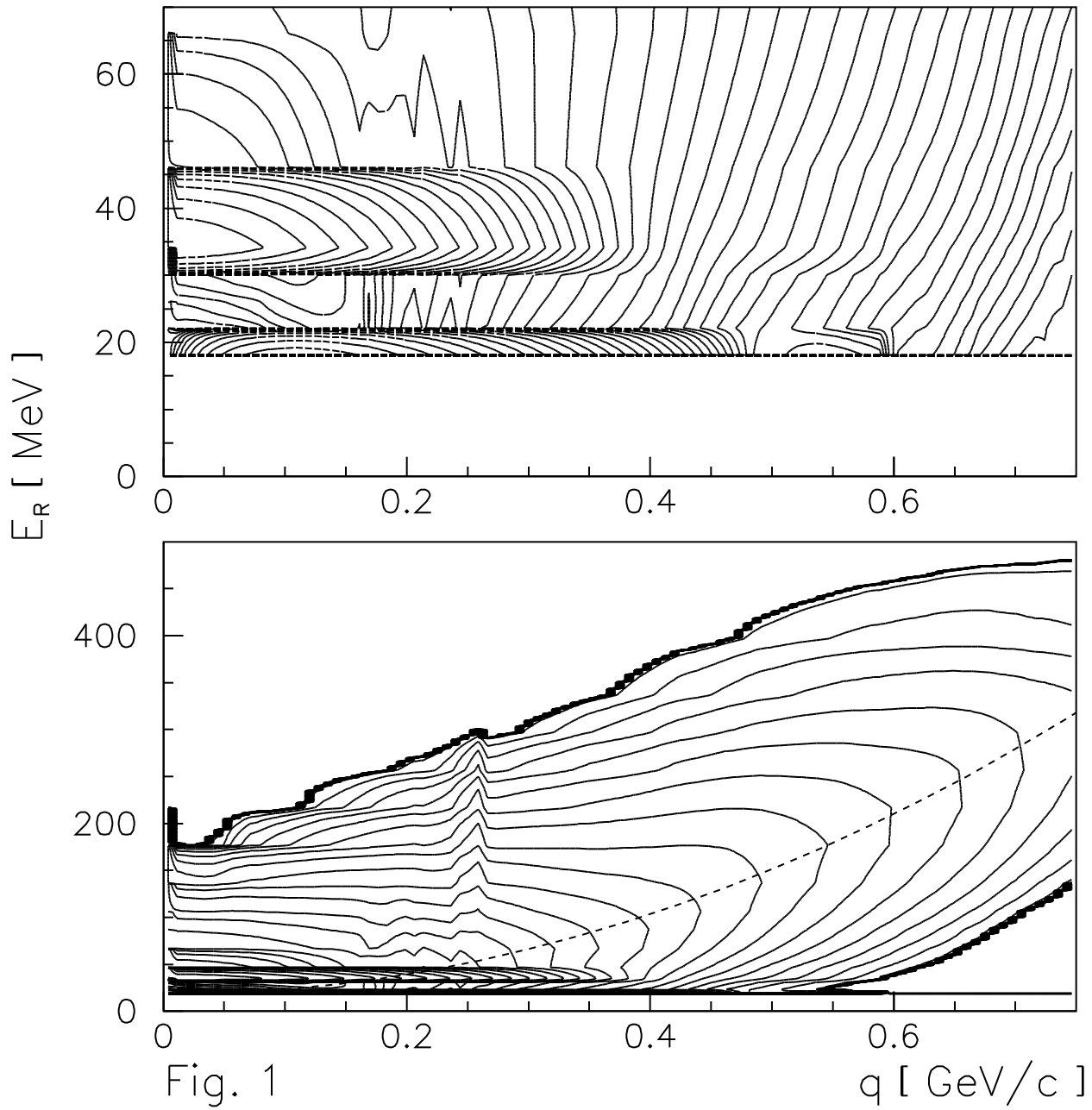
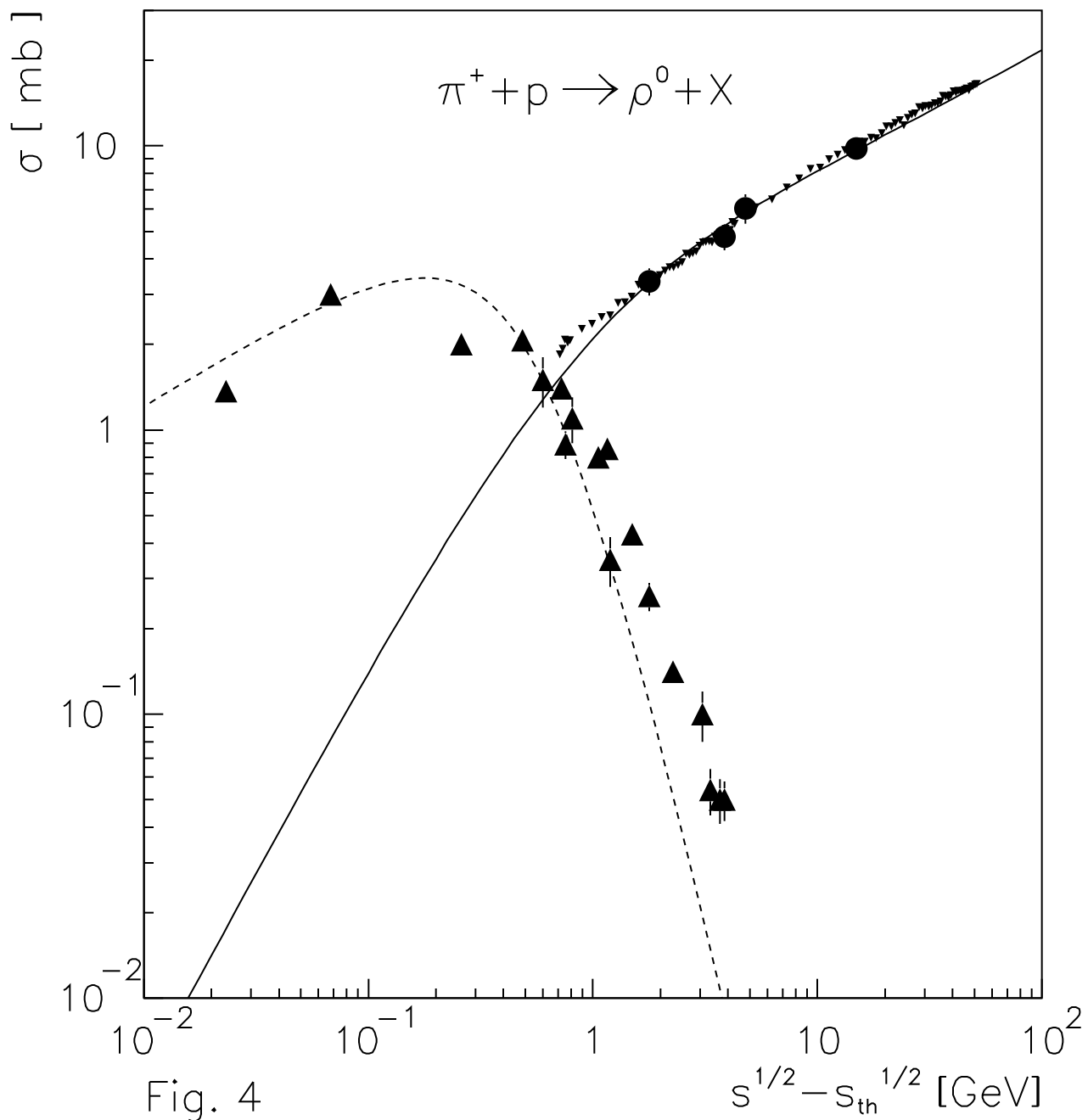


Fig. 1

$q$  [ GeV/c ]





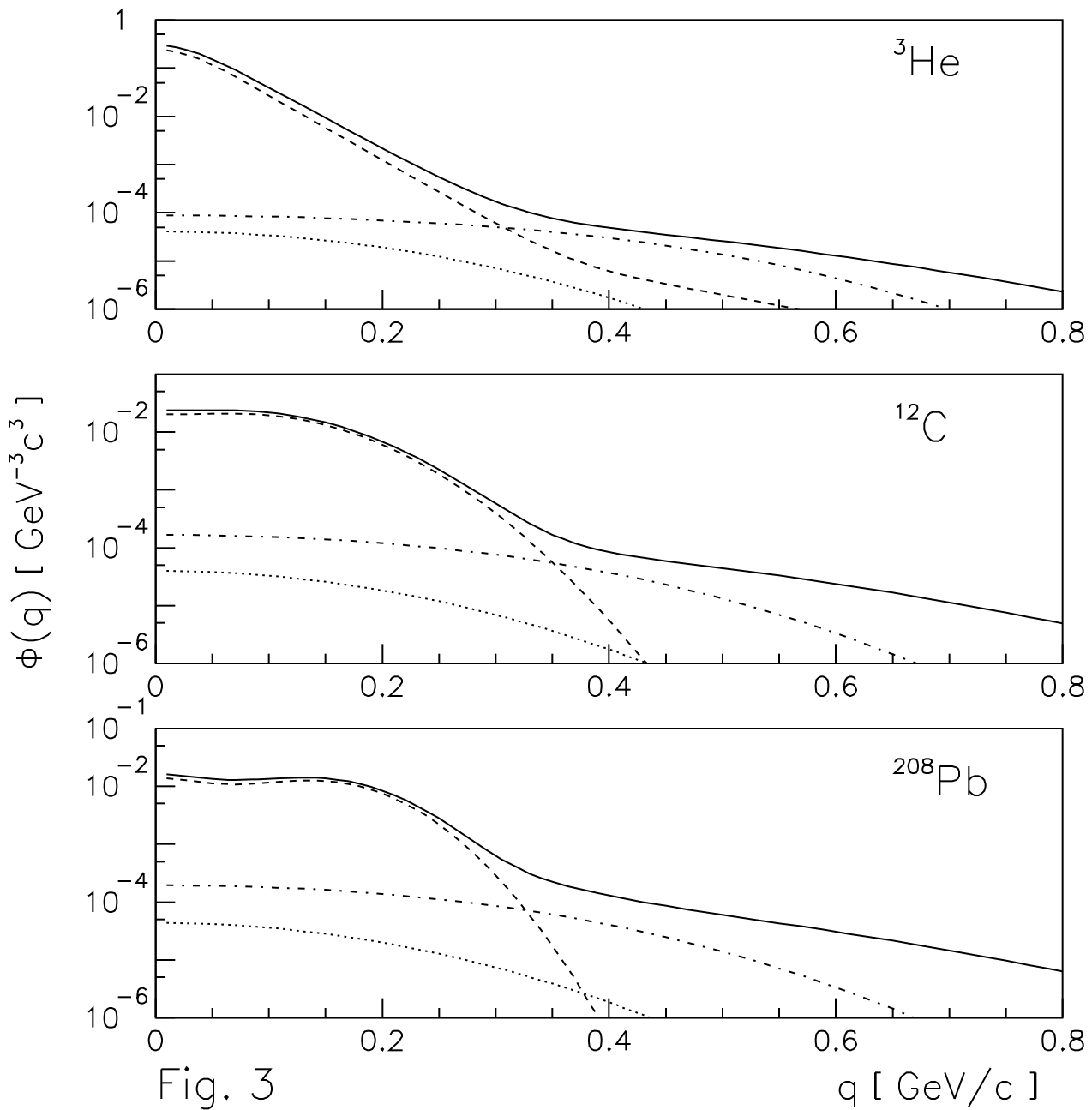
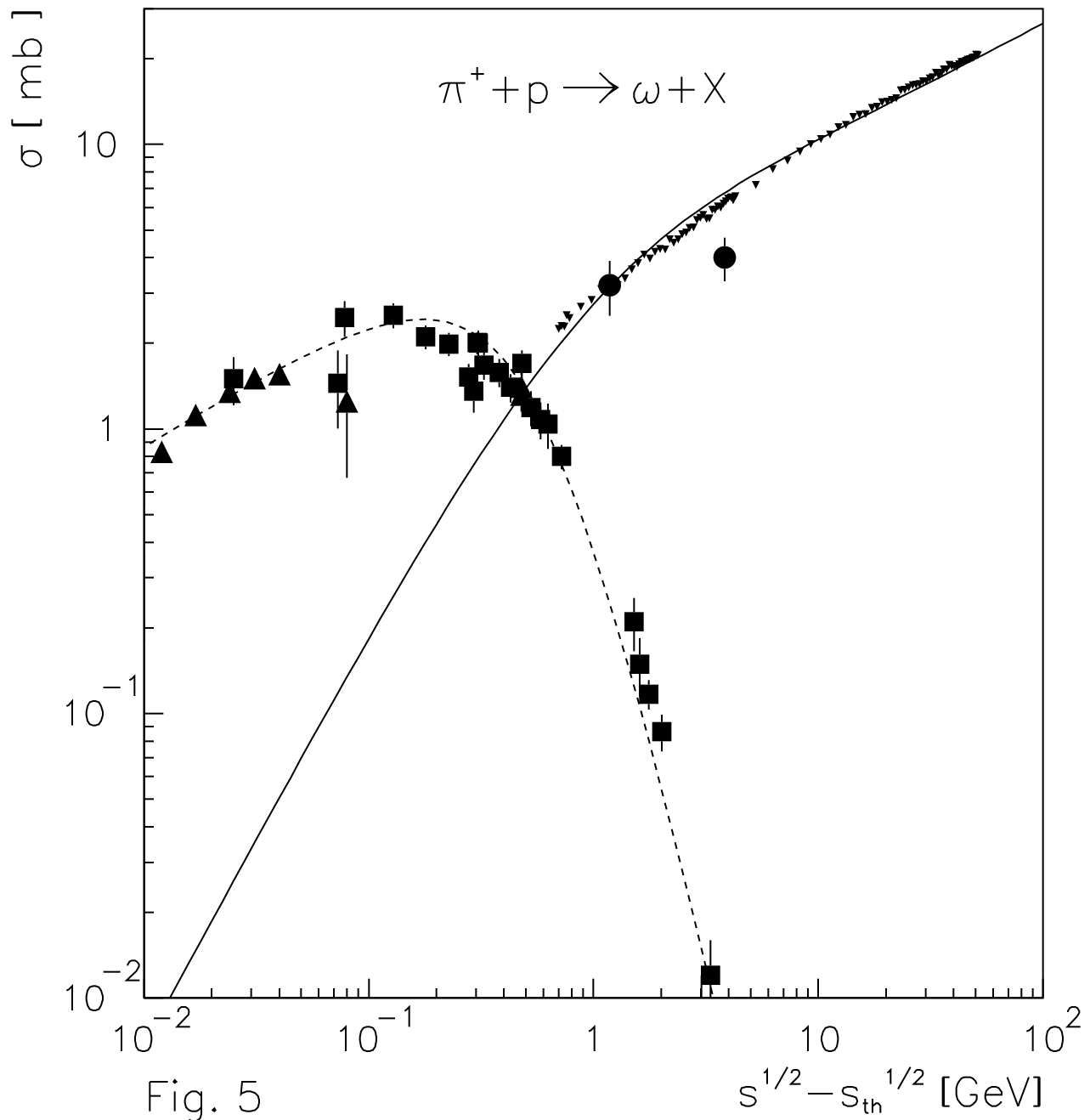


Fig. 3

$q$  [  $\text{GeV}/c$  ]



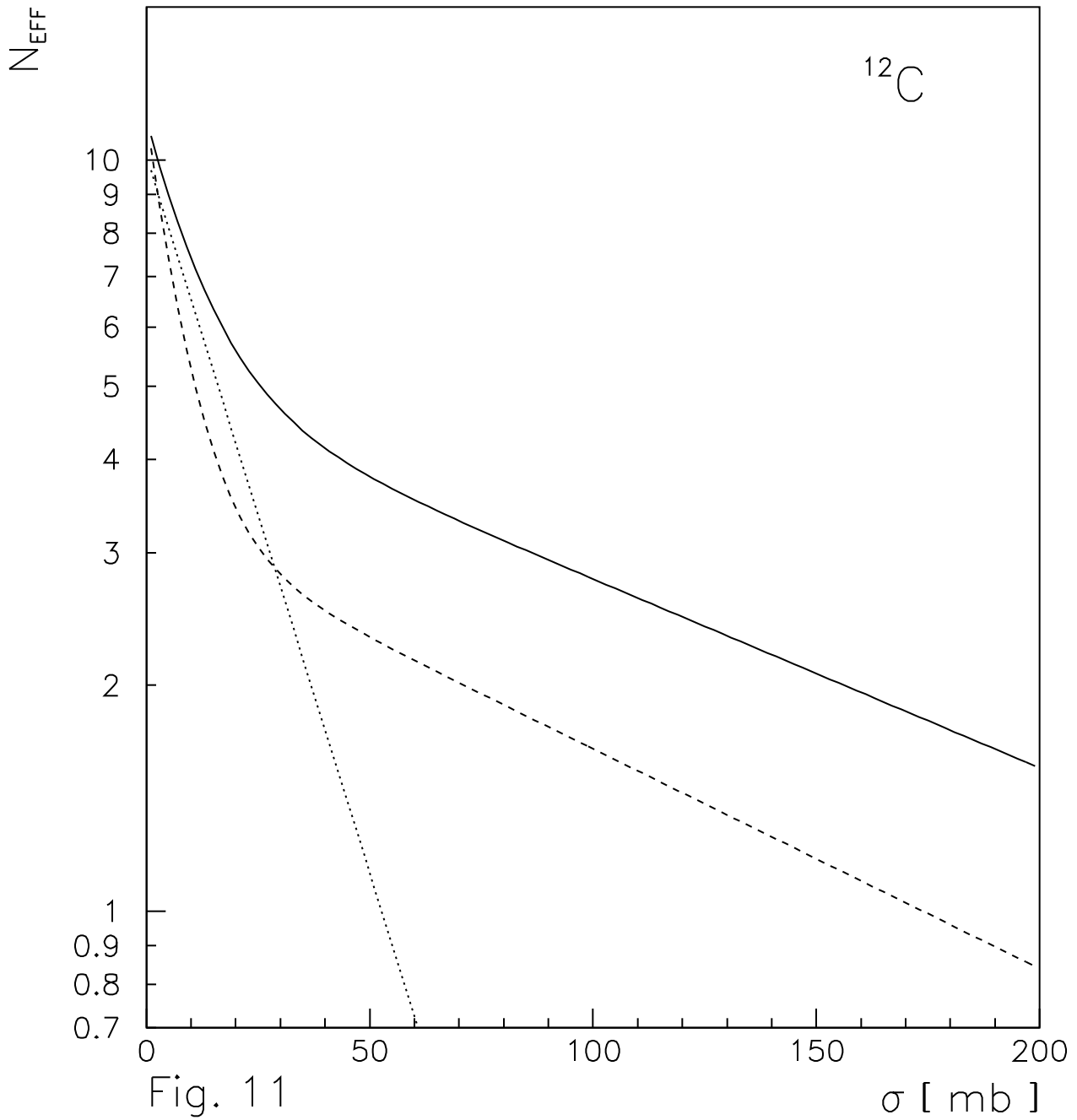


Fig. 11

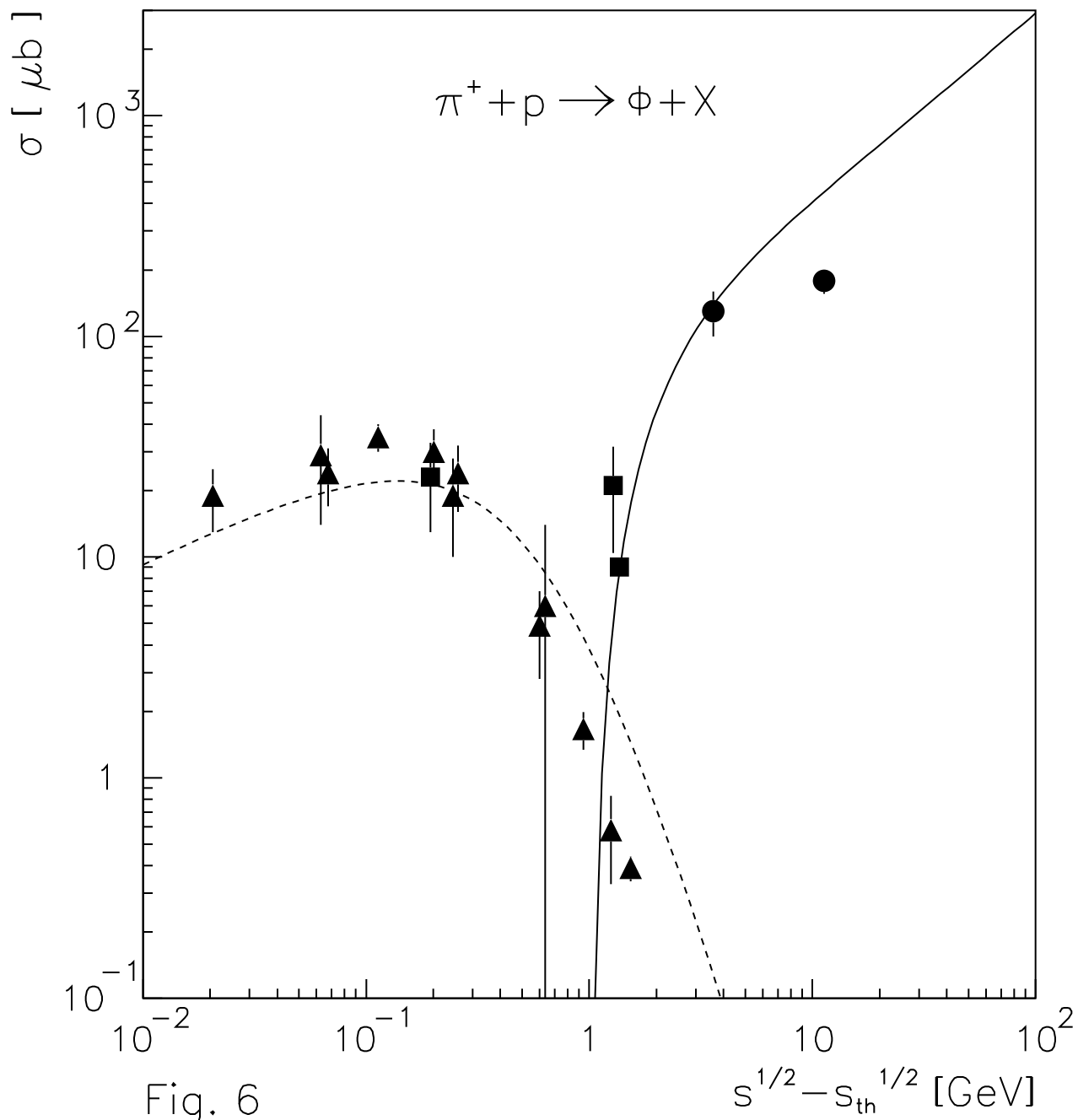


Fig. 6

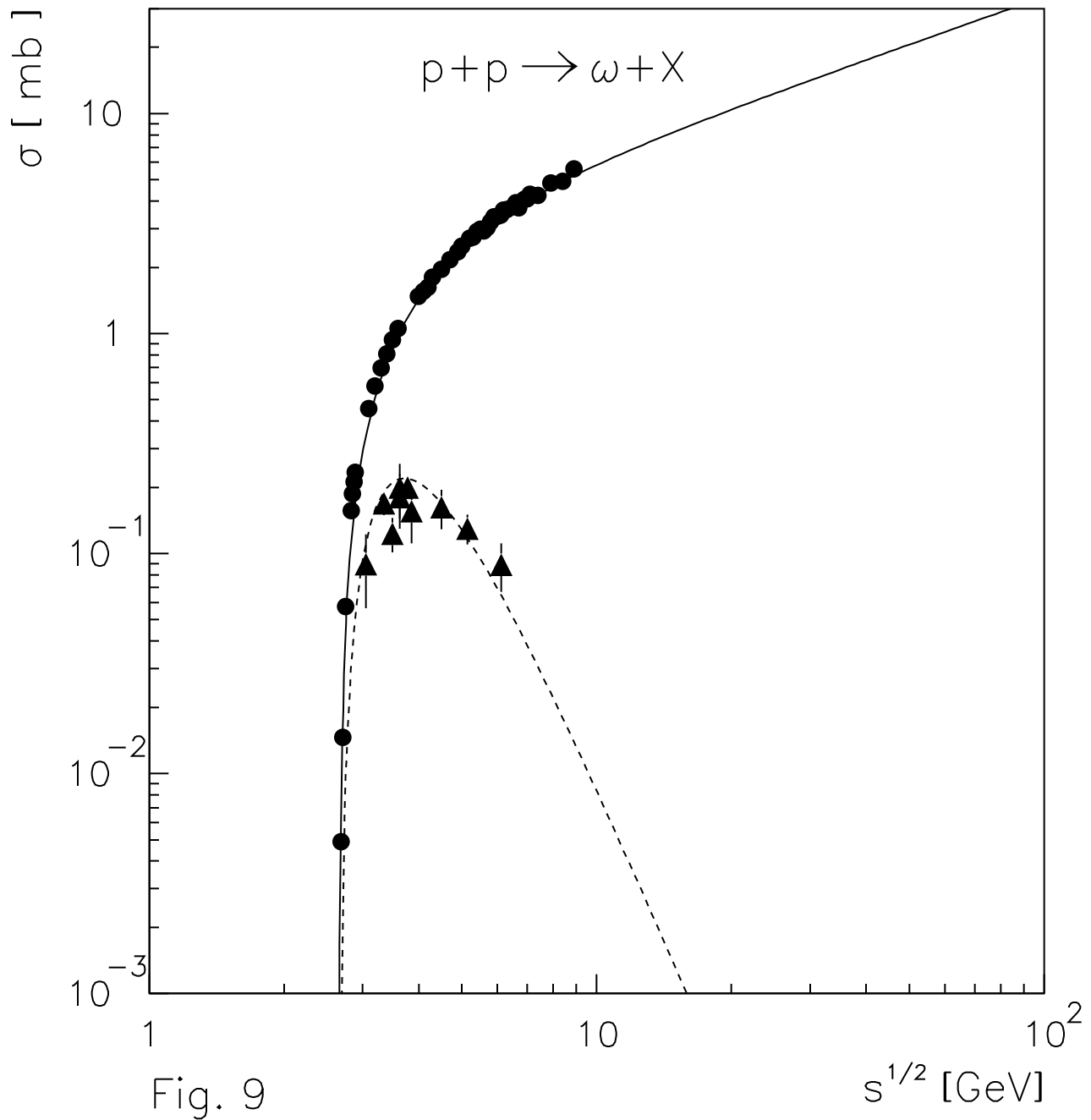


Fig. 9

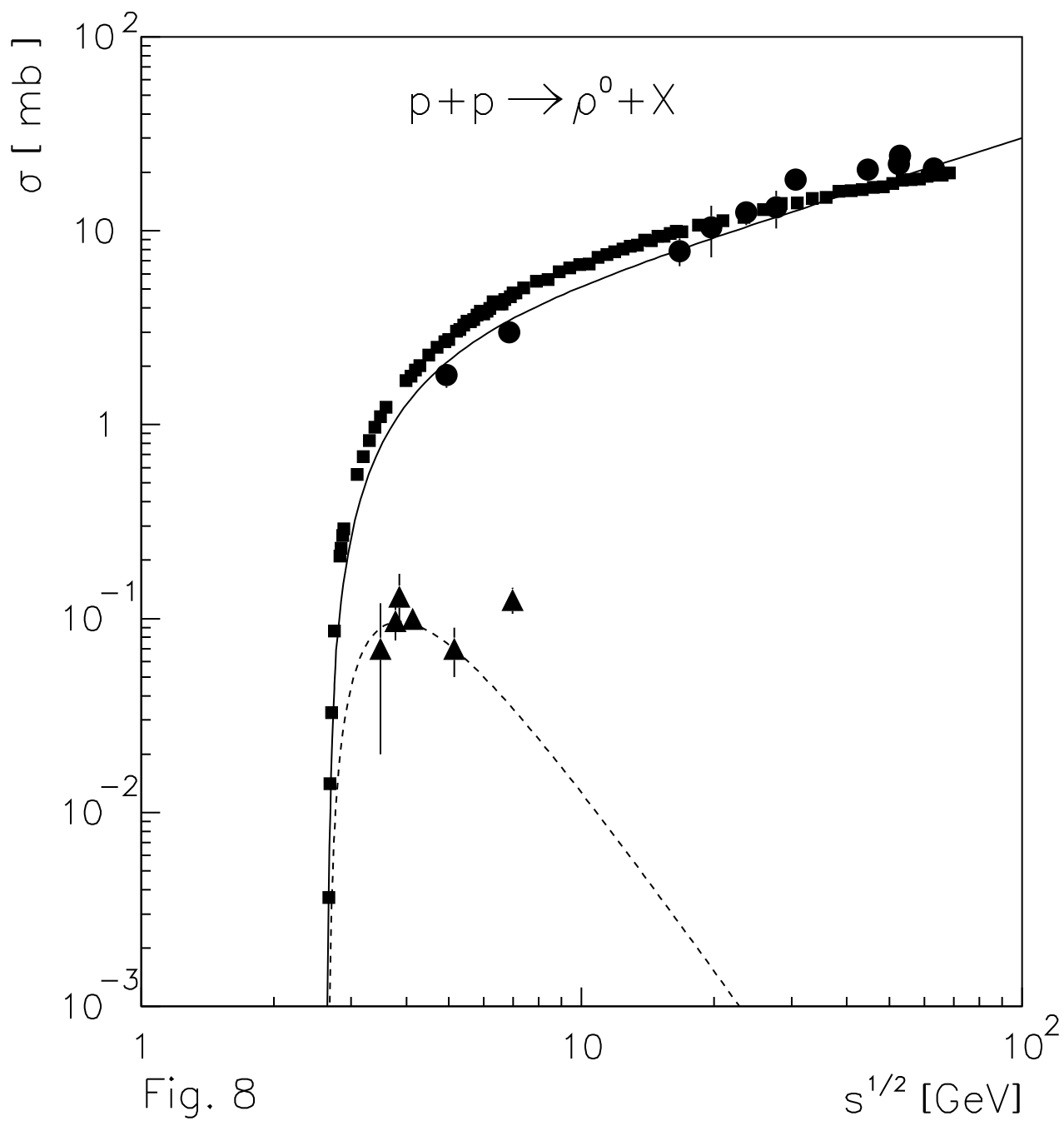


Fig. 8

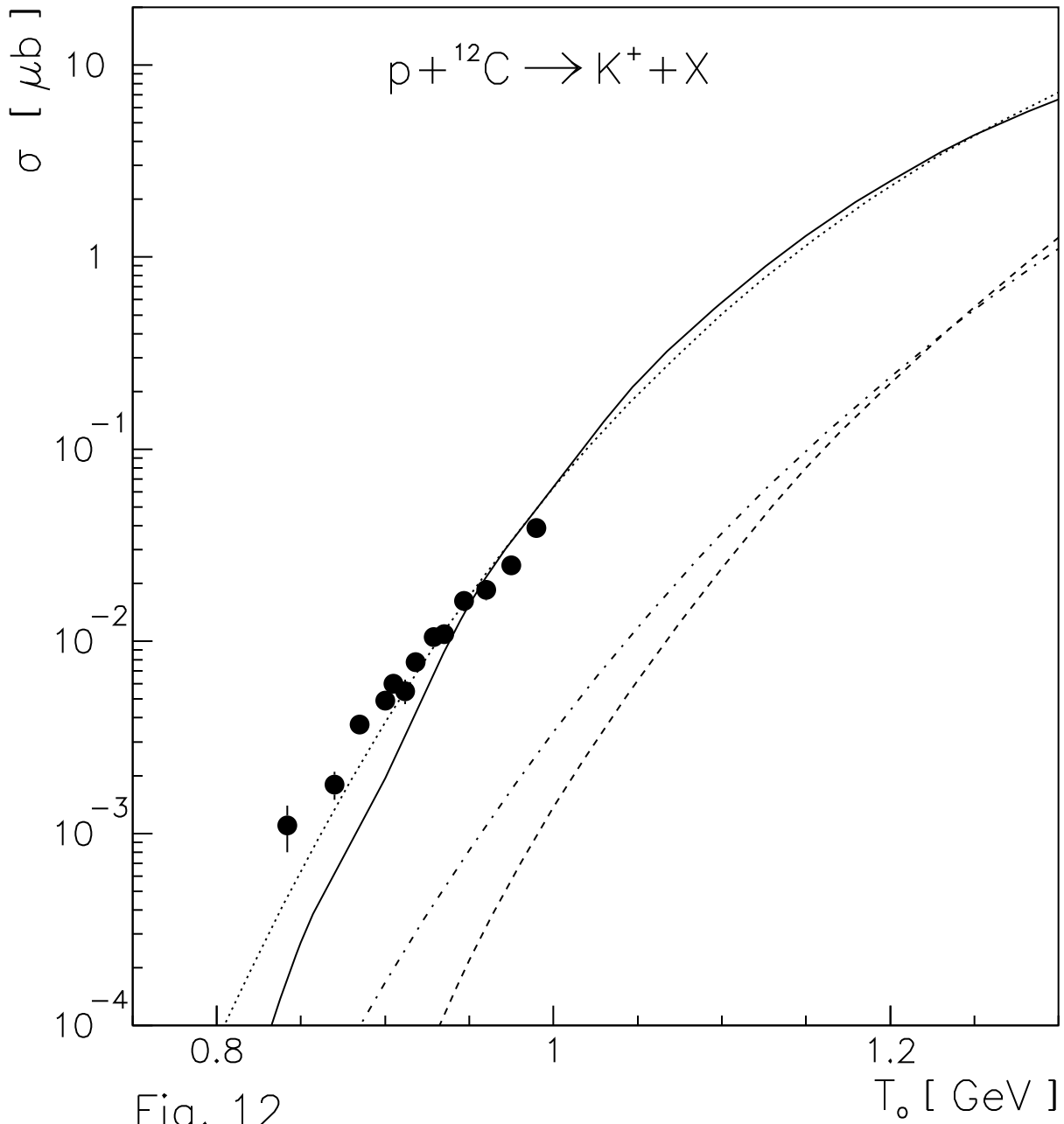


Fig. 12

